PHYSICAL REVIEW D **91,** 044034 (2015)

Fundamental oscillation modes of neutron stars: Validity of universal relations

Cecilia Chirenti,[1*] Gibran H. de Souza,[2] and Wolfgang Kastaun[3]

[1]*Centro de Matemática, Computação e Cognição, UFABC, 09210-170 Santo André-SP, Brazil*
[2]*Instituto de Física Gleb Wataghin, UNICAMP, 13083-859 Campinas-SP, Brazil*
[3]*Physics Department, University of Trento, via Sommarive 14, I-38123 Trento, Italy*

(Received 13 January 2015; published 19 February 2015)

We study the f-mode frequencies and damping times of nonrotating neutron stars (NS) in general relativity by solving the linearized perturbation equations, with the aim to establish "universal" relations that depend only weakly on the equations of state (EOS). Using a more comprehensive set of EOSs, we reexamine some proposed empirical relations that describe the f-mode parameters in terms of mass and radius of the NS, and we test a more recent proposal for expressing the f-mode parameters as quadratic functions of the effective compactness. Our extensive results for each equation of state considered allow us to study the accuracy of each proposal. In particular, the empirical relation proposed in the literature for the damping time in terms of the mass and radius deviates considerably from our results. We introduce a new universal relation for the product of the f-mode frequency and damping time as a function of the (ordinary) compactness, which proved to be more accurate. The more recently proposed relations using the effective compactness, on the other hand, also fit our data accurately. Our results show that the maximum oscillation frequency depends strongly on the EOS, such that the measurement of a high oscillation frequency would rule out several EOSs. Lastly, we compare the exact mode frequencies to those obtained in the Cowling approximation, and also to results obtained with a nonlinear evolution code, validating the implementations of the different approaches.

DOI: 10.1103/PhysRevD.91.044034 PACS numbers: 04.30.Db, 04.40.Dg, 95.30.Sf, 97.60.Jd

I. INTRODUCTION

Neutron stars are among the most interesting celestial objects since their description requires both general relativity and nuclear physics. The state of matter in the core of neutron stars (NSs) is not accessible to any terrestrial experiments, and thus provides a unique laboratory to test theoretical predictions for matter at high densities and relatively low temperatures (compared to particle collisions producing comparable energy densities). In particular, there exist many different models predicting the equation of state (EOS) of NS matter, see [1–11], among others. A possibility to constrain those models from NS observations is given by the fact that general relativity predicts a maximum mass for nonrotating and uniformly rotating NSs, which depends on the EOS. Recently, [12] and [13] discovered NSs with masses as high as $1.97M_\odot$ and $2.01M_\odot$, respectively. This already ruled out several EOSs, as shown in Fig. 1. A simultaneous observation of mass and radius of a slowly rotating NS would serve the same purpose.

Given a set of observed quantities, constraining the EOS obviously requires relations which do depend strongly on the EOS. On the other hand, relations which do *not* depend on the EOS (or only weakly), are highly useful as well, since they would allow us to constrain further unknown parameters without knowledge of the EOS. Such universal relations have already been established in the context of binary NS evolution between moment of inertia, the tidal deformability (Love number) and the quadrupole moment, both for regular NSs and quark stars, see [14–16]. Weakly EOS dependent relations between compactness and normalized moment of inertia have been found by [17,18].

Other studies [19–22] have investigated various empirical universal expressions for oscillation frequencies and

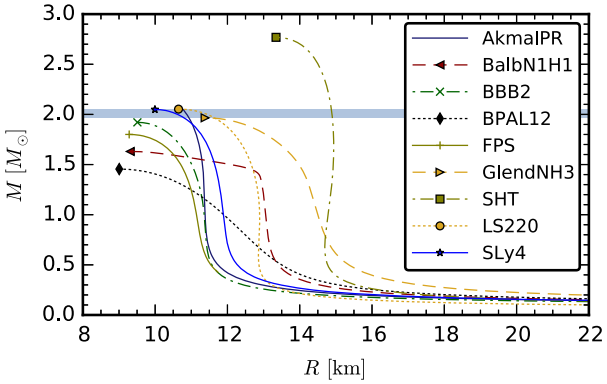

FIG. 1 (color online). Gravitational mass M versus circumferential radius R for the set of EOS used in this work. The shaded area shows the mass range measured by [13] for the pulsar PSR J0348 + 0432. The symbols mark the maximum mass models.

*cecilia.chirenti@ufabc.edu.br

damping time scales. Among the various types of oscillation modes, the main focus has been on modes for which pressure is the restoring force, in particular the fundamental modes (f modes). Knowledge of the f modes of nonrotating stars also provides estimates for the f-mode properties of slowly rotating stars, for the case of uniform rotation [23] and also for differential rotation [24].

Some years ago, Andersson and Kokkotas [19] proposed an empirical relation for the f-mode oscillation frequency ω, based on Newtonian theory of stellar perturbations. They observed that in full GR, ω depends almost linearly on the square root of the average density. Another relation, based on estimates using the quadrupole formula, was established for the damping time due to gravitational wave emission, τ. Later, Benhar *et al.* [20] presented further results that included more and newer equations of state, updating the fits from [19]. The average frequencies ω were systematically lower than the one for the old EOS sample, which they attributed to the fact that the new sample included stiffer EOSs.

This highlights an important point: all the universal relations are not truly EOS-independent, but restrain parameters in a relatively narrow band which depends on the EOSs taken into account. Using this band to interpret observational data implicitly assumes that the true EOS is similar to one of the EOSs considered. It is therefore important to include a large range of EOSs in the sample, to prevent underestimating the residual uncertainties due to the EOS. For this reason, we do not exclude EOSs already ruled out by the observation [13].

More recently, Lau *et al.* [21] improved on the results from [22] by using quadratic fits for both ω and τ. Further, they use the "effective compactness" $\eta \equiv \sqrt{M^3/I}$ as independent variable, where I is the moment of inertia. In contrast to measures involving the surface radius, η is determined by the bulk properties of the NS. Note the moment of inertia could be constrained for isolated stars by observations of spindown and energy output due to magnetic braking, see [17]. It might also be measured from high precision observations of spin-orbit couplings in a binary pulsar system, see [18].

Observing oscillations of isolated NSs might in principle be possible through conventional astronomy if they are equipped with a magnetic field. The direct production of electromagnetic emissions due to NS (and BH) perturbations was investigated in [25,26]. Stellar oscillations might also modulate EM emissions produced by other processes. For example, possible signatures of NS oscillations have already been observed in the luminosity curves of magnetar giant flares [27]. However, the low frequencies rule out fundamental modes as the cause. Instead, the modulation was attributed to oscillations of the magnetar crust and magnetic field, see [28] and the references therein.

Another observational channel is given by the gravitational waves emitted by oscillating NSs, which have been the subject of many studies over the years (see [29–31] and references therein). The detection range is however limited by the fact that oscillations above a certain amplitude are strongly damped by nonlinear effects [32]. Moreover, possible excitation mechanisms most likely already saturate at much lower amplitudes. The most famous mechanism is the Chandrasekhar-Friedman-Schutz instability [33], which is restricted to rapidly rotating NSs (for the case of f modes), and probably suppressed by superfluid or viscous effects outside the instability window described in [34]. More speculative excitation mechanisms are phase transitions of the EOS [35], or resonant excitation in eccentric binaries, proposed by [36] (although it seems questionable whether the binary stays in the resonant window sufficiently long).

The most promising source of detectable gravitational waves (GW) from NSs is given by the hyper- or supramassive neutron stars which can be formed in binary NS mergers [37]. However, those are rapidly and differentially rotating. Further, they are hot and not in β-equilibrium, and thus do not follow a simple barotropic EOS. Due to these additional degrees of freedom, universal relations found for slowly rotating cold stars are not directly applicable. Still, a better understanding of the simple nonrotating case is certainly beneficial for the development of more sophisticated models needed to describe hypermassive NSs.

Our first aim in this paper is to provide accurate results for the f modes in a wide range of masses and the EOSs given in Table I, which we hope will be useful for the community. In spite of being widely used in this field, properties of the f modes are not available in the literature for some of the EOSs.

Our second aim is to update the empirical relations studied in [19] and [20], and test the proposed universal relations from [21] for the newer EOS we consider here. This analysis is presented in Sec. II.

In Sec. III, we compare our linear results to nonlinear, fully relativistic 3D simulations of selected models. We also study the (in)accuracy of the relativistic Cowling approximation for selected EOSs. Finally, we present our concluding remarks in Sec. IV. Numerical results for all equations of state considered here are provided in the Appendix.

TABLE I. The equations of state used in this paper. All of the EOS, except for the last two, are distributed with the publicly available Lorene code [38]. The LS220 and SHT EOSs include temperature and composition dependency; we use the barotropic EOSs obtained by imposing zero-temperature and β-equilibrium.

EOS	Ref.	EOS	Ref.	EOS	Ref.
AkmalPR	[2]	BPAL12	[5]	SLy4	[8,9]
BalbN1H1	[3]	FPS	[6]	LS220	[10]
BBB2	[4]	GlendNH3	[7]	SHT	[11]

II. NUMERICAL RESULTS FOR THE f-MODE FREQUENCIES AND DAMPING TIMES

Our numerical scheme for obtaining the f-mode frequencies and damping times solves the set of perturbation equations derived in the original papers by Lindblom and Detweiler [39,40], based on the pioneering work by Thorne and collaborators [41–46]. Our algorithm follows closely the outline given in [39,40], and some preliminary results obtained for a polytropic EOS were presented in [47]. We solve the eigenvalue problem using the Newtonian f-mode frequency as an initial guess. The radial perturbation equations inside the star, written as a system of 4 coupled ODEs, are solved with a standard 4th order Runge-Kutta method. The solution obtained is then matched to the numerical solution of the Zerilli equation at the surface and to the asymptotic solution of the Zerilli equation at a large enough radius. Finally, we use a shooting method to refine the initial guess and determine the complex eigenfrequency, by imposing the purely outgoing wave condition at infinity.

Our code assumes that the EOS of the background model is also valid to describe dynamic perturbations. This is an approximation since the system can deviate from β-equilibrium. To estimate the importance of this error, we compare the speed of sound for two corner cases: c_s^β is the sound speed assuming that β-equilibrium is always satisfied, and c_s^Y is the sound speed assuming that the electron fraction is fixed along fluid world lines. We define an average relative error of the sound speed by $\bar{\delta}c_s = \sqrt{(\int \delta c_s^2 \rho \mathrm{d}\rho)/(\int \rho \mathrm{d}\rho)}$, with $\delta c_s = 1 - c_s^\beta / c_s^Y$. Of our EOS sample only the LS220 and SHT EOSs provide values out of β-equilibrium. For both, we find $\bar{\delta}c_s \approx 1\%$. Since stellar oscillations are strongly related to the sound crossing time, and assuming the frequencies are mainly determined by the bulk of the star, we use $\bar{\delta}c_s$ also as a rough estimate for the corresponding differences of the oscillation frequencies. As an independent measure, we note radial oscillation frequencies of NS have been compared in [48] for the two corner cases above, using the same EOSs. The resulting frequencies differ by $\approx 1\%$, in agreement with the estimate above. Since the GW luminosity depends on the frequency, we can expect similar differences for the damping time. For the rest of this article, we will ignore the influence of the β-equilibrium assumption. The purely numerical error in the determination of the f-mode parameters is approximately 0.1% for ω and 2% for τ. This was estimated by running convergence tests with 5000, 10000, and 20000 points for different models spanning the whole mass range.

In the following, we present our numerical results and compare them with the empirical relations presented by Andersson and Kokkotas [19], Benhar *et al.* [20] and Lau *et al.* [21]. Our selection of EOSs given in Table I differs from the ones used in those works in that we have more EOSs than [20] and newer EOSs that were not considered in [19] and [21] (we do not consider here some of their older EOSs nor quark matter). We also include the LS220 and SHT EOSs which are frequently used in merger simulations. For each EOS, we set up models in a large mass range, starting from $1M_\odot$ up to the maximum mass. We sample the corresponding central energy density range linearly, using 101 data points for each EOS. Note for the AkmalPR EOS, the central sound speed becomes superluminal at a density below the one of the maximum mass model. We excluded all the causality-violating models. Following [19] and [20], we used the data from all the EOS to fit the empirical relations below, which relate the f-mode frequency ω to the square root of the average density M/R^3, and the damping time τ to the compactness M/R of the neutron star:

$$\omega = a_1 + b_1 \sqrt{\frac{M}{R^3}}, \tag{1}$$

$$\frac{R^4}{M^3 \tau} = a_2 + b_2 \frac{M}{R}. \tag{2}$$

These relations are shown in Fig. 2. As one can see, each EOS individually satisfies a linear relation given by Eq. (1) to good accuracy. There is however a considerable spread between the different EOSs. We fitted Eq. (1) to all models combined to get an average relation. Since the spread is of systematic nature, the formal statistical errors of the fit are meaningless. We stress that the fit result itself is also ambiguous, since it depends on the selection of models and there is no "true" value. Our aim is to establish a band around the fitted relation which contains all our results, and which can be used to constrain observational data without detailed knowledge of the EOS, only assuming that it is similar to one of the EOSs from our sample. To define this "confidence band," we simply use the largest residual of the fit as systematic error of the constant offset a_1. Our fit results for Eq. (1) are given in Table II. The table also contains the results of the same fit applied to each EOS individually, which can be used to estimate oscillation frequencies for a given EOS to good accuracy. The fits from [19] and [20], also shown in Fig. 2, are also contained within the confidence band that envelopes our results. The differences between [19] and [20], attributed to the different sets of EOSs used in the two studies, are smaller than the spread between the individual EOSs we considered.

For the damping times, also shown in Fig. 2, we fitted Eq. (2) to our data, obtaining values $a_2 = 0.084 \pm 0.012$, $b_2 = -0.260$, where the error given for a_2 is the largest residual. The differences between our result and the fits from [19] and [20] are smaller than the spread between the different EOSs, and thus compatible. However, as visible in Fig. 2, a linear relation does not describe the data well in the larger compactness range we consider. Although this could be compensated by fitting a more appropriate curve, there is

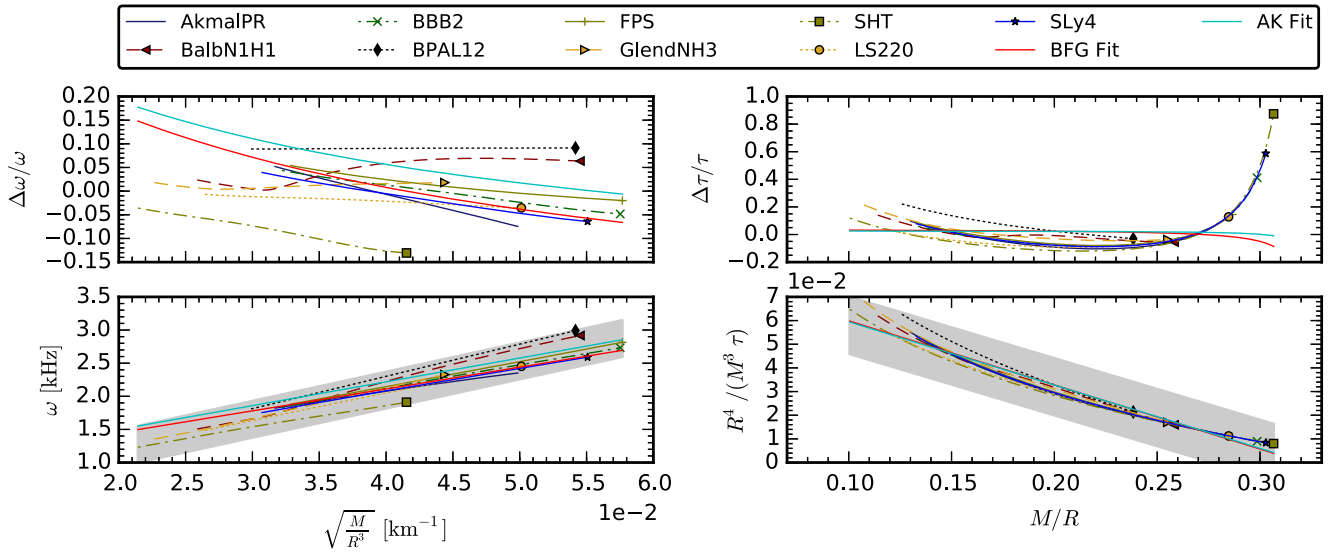

FIG. 2 (color online). Properties of the f mode in terms of mass and radius, and EOS-independent approximations. The left panels show the relation Eq. (1) for the frequency, the right panels the relation Eq. (2) for the damping time. The lower panels show the exact results for each EOS as well as the fits proposed in [20] (BFG) and [19] (AK). The shaded regions show the confidence bands (see main text) around our fits. The upper panels show the remaining EOS dependency in terms of the residuals of our fit, as well as the differences to the AK and BFG fits.

also a large spread between the different EOS. The spread and the deviation from linearity strongly limits the usefulness of Eq. (2) for constraining observational data.

Next, we tested the universal relations proposed in [21], which express the f-mode properties in terms of the effective compactness η. In particular, we fit the expression

$$M\omega = a_3 + b_3\eta + c_3\eta^2 \tag{3}$$

for the frequency to our results for all EOSs. We find values $a_3 = -0.00383 \pm 0.0022$, $b_3 = 0.1276$, and $c_3 = 0.5718$. The error provided for a_3 defines a confidence band which contains the results for all our models as well as the fit provided[1] in [21]. This takes into account that some of the EOSs used in [21] are not part of our EOSs sample. The fit results are shown in Fig. 3. As one can see, the universal relation proposed in [21] describes the results for our set of EOSs and models still very well.

In order to parametrize the damping time, we fit the expression

$$\frac{I^2}{M^5\tau} = a_4 + b_4\eta^2, \tag{4}$$

proposed in [21], to our models. We obtain values $a_4 = 0.00680 \pm 0.00013$ and $b_4 = -0.0250$. The error given for a_4 again defines a band containing all our models as well as the fit provided in [21]. The results are plotted in Fig. 3, showing that the universal relation for the damping time holds to good accuracy for our models.

We note that the relation between compactness and effective compactness is also weakly EOS dependent, as pointed out in [17,18], where the normalized moment of inertia $\tilde{I} = I/(MR^2)$ is given as a function of compactness M/R. This can easily be rearranged in terms of effective compactness η and compactness M/R. For the EOSs considered here, the resulting relation is shown in Fig. 4. Compared to the empirical fit proposed by [18], our models have a slightly larger effective compactness on average.

TABLE II. Parameters a_1, b_1 of the linear fit given by Eq. (1) applied to each EOS individually, and to all models combined. $\Delta\omega$ denotes the largest residual. For comparison, we also include the fits from [19] (AK Fit) and [20] (BFG Fit).

Model	a_1 [kHz]	b_1 [kHz km]	$\Delta\omega$ [kHz]
AkmalPR	0.912	29.05	0.011
BalbN1H1	0.116	52.08	0.043
BBB2	0.705	35.33	0.013
BPAL12	0.355	48.65	0.001
FPS	0.634	37.78	0.005
GlendNH3	0.295	45.79	0.022
SHT	0.542	32.98	0.018
LS220	0.419	40.65	0.008
SLy4	0.713	34.13	0.008
Combined	0.332	44.04	0.275
BFG Fit	0.790	33.00	...
AK Fit	0.780	35.96	...

[1]Note there is a typo in Eq. (6) from [21], where the last coefficient should read 0.575 instead of 0.0575 in order to be consistent with their Fig. 1.

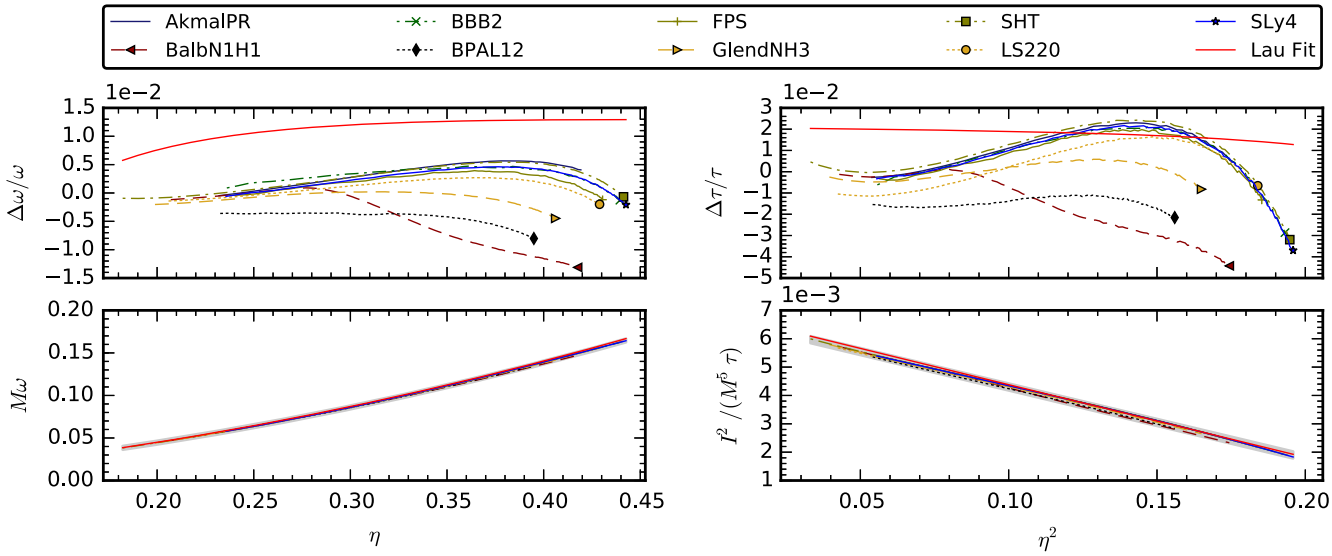

FIG. 3 (color online). Universal relations of the f mode in terms of the effective compactness and mass. The left panels show the relation Eq. (3) for the frequency, the right panels the relation Eq. (4) for the damping time. The lower panels show the exact results, where the shaded area depicts the confidence bands containing all models (see main text). The upper panels show the deviations from our fit. For comparison, we also plot the fits provided in Lau *et al.* [21].

In [21], it was proposed to use the relations given by Eqs. (3) and (4) to estimate mass and effective compactness from measurements of ω and τ, and further to compute the radius using the aforementioned universal relation between η and compactness. The resulting mass and radius could in principle be used to constrain the EOS, although the remaining EOS dependency of the "universal" relations used for the estimate could be prohibitive. To decide whether a simultaneous observation of frequency and damping time can really restrict the EOS, it is easier to simply plot the damping time as a function of frequency for all EOSs, as shown in Fig. 5. As one can see, there is a considerable overlap between the curves for different EOSs. Nevertheless, the maximum oscillation frequency, which is in general reached for the maximum mass model, depends strongly on the EOS. A measurement of a high frequency could thus rule out many EOSs, even without knowledge of the damping time. The frequencies of the maximum mass models can be found in the Appendix.

We also observe that the minimum damping time depends on the EOS. The measurement of a short damping time scale would in principle constrain the EOS, even without knowledge of the frequency. In practice however, the damping is probably not caused by GW emission alone, in particular at high amplitudes. Thus the observed damping time would only be a lower limit for the radiation reaction time, and hence not constrain the EOS.

Searching for a better relation for the damping time in terms of compactness, we turned to the dimensionless quantity $\omega\tau$. Multiplying by the frequency is not a serious drawback since for any observation long enough to

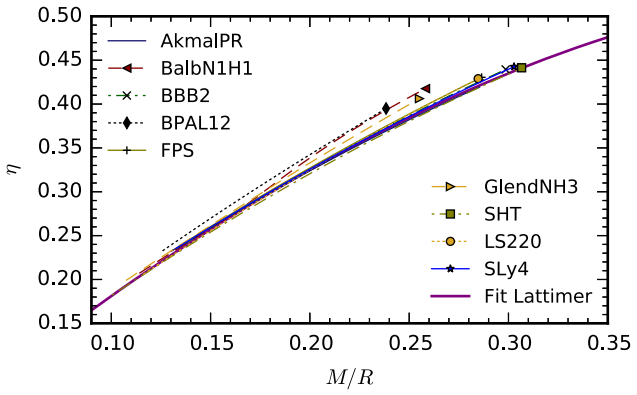

FIG. 4 (color online). Effective compactness η versus compactness for all EOSs. In addition, we show the fit given in [18].

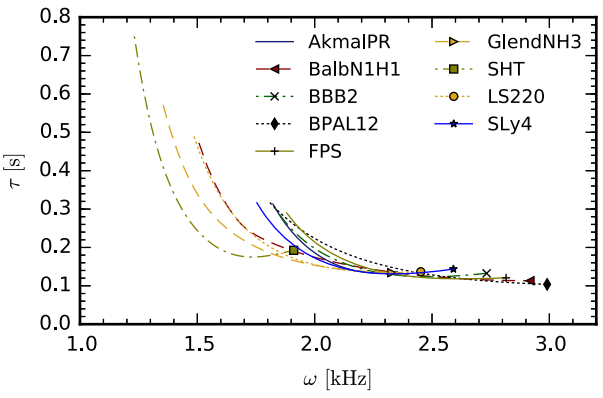

FIG. 5 (color online). Damping time due to GW emission versus oscillation frequency for all EOSs. The symbols mark the maximum mass models, which also exhibit the largest frequency.

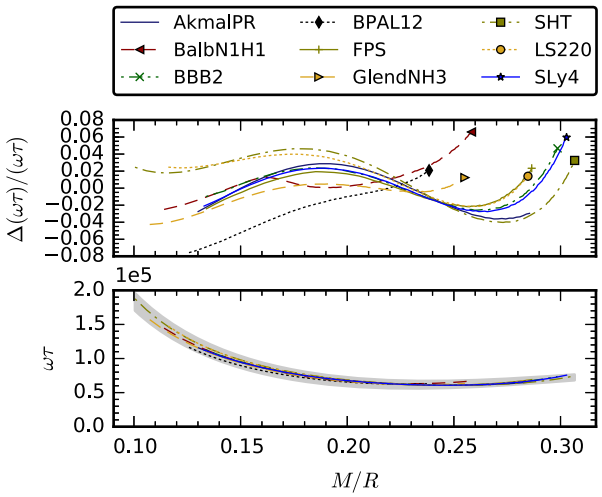

FIG. 6 (color online). Universal relation for the dimensionless quantity $\omega\tau$ in terms of compactness. The lower panel shows the exact values for all EOSs together with the confidence band around the fitted value (see main text). The upper panel shows the deviation from the fitted relation.

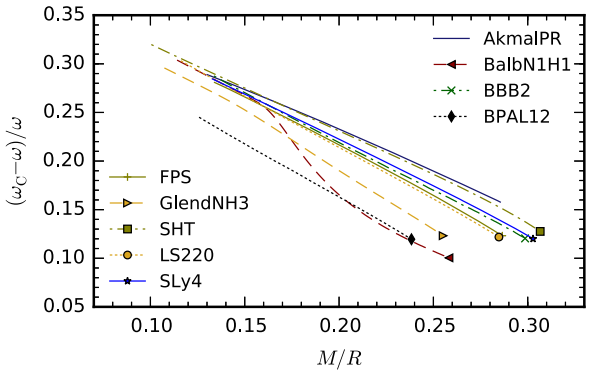

FIG. 7 (color online). The relative difference between f-mode frequencies obtained in full GR and the Cowling approximation.

determine the damping time, the frequency will also be known to good accuracy. The choice is motivated by the fact that for a subset of EOS given by polytropic EOSs with fixed polytropic index, but arbitrary polytropic constant, all relations expressed in terms of quantities which are dimensionless in geometric units are automatically universal. Note the fits given by Eqs. (3) and (4) are already in terms of dimensionless quantities. Although realistic EOS do not exhibit the underlying scaling invariance of polytropes, we found that our data is well represented by the relation

$$\omega\tau\frac{M}{R} = a_5 + b_5\frac{M}{R} + c_5\left(\frac{M}{R}\right)^2 \tag{5}$$

with $a_5 = (3.69 \pm 0.129) \times 10^4$, $b_5 = -2.50 \times 10^5$, $c_5 = 6.59 \times 10^5$. The error given for a_5 denotes the largest residual. The fit is shown in Fig. 6. Although $\omega\tau$ is well constrained by the compactness, the relation can only be inverted for low compactness. It is therefore of limited use for constraining the compactness from a measurement of $\omega\tau$.

III. COMPARISON WITH DIFFERENT METHODS

In this section we study the accuracy of the Cowling approximation with respect to f modes and compare our results to three-dimensional nonlinear numerical simulations.

A. Cowling approximation

We now compare the frequencies obtained in full GR, presented in Sec. II, to those obtained using the Cowling approximation, which neglects the metric perturbations. Keeping the gravitational field fixed leads to significant changes in the mode frequencies, see [23,49]. Further, there is no emission of gravitational waves and one obtains normal modes of oscillation, instead of decaying quasi-normal modes.

In order to obtain the frequencies in the Cowling approximation, we use a semianalytic code case based on the linearized equations given in [50], assuming harmonic time dependence and specializing to spherical symmetry. The resulting singular boundary value problem for the eigenfunctions is solved using the method of Frobenius to compute the solution at the boundaries (origin and surface) in conjunction with a shooting method to determine the mode frequency.

The relative difference for all the EOS considered here is displayed in Fig. 7. Our comparison matches the conclusions presented in [23]: the difference ranges from ≈10–30% and decreases with increasing stellar compactness. A possible explanation for this trend was proposed by [51], noting that increasing compactness can make the role of metric perturbations less relevant for the f-mode eigenfunction, given that the eigenfunction is peaked near the surface.

B. Numerical relativity simulations

As an additional cross check, we compare our linear results (both GR and Cowling) to those obtained with a nonlinear, three-dimensional numerical evolution code. The nonlinear results are more expensive and, due to limited resolution, less accurate, but they are completely independent both regarding the analytic formalism and the numerical implementation. Note that the numerical damping typical for such codes prevents the computation of the physical damping time scale associated with GW radiation, which is why we only compare the frequencies.

The nonlinear hydrodynamic evolution code is described in [48]. It is based on a conservative formulation of the hydrodynamic evolution equations, which are solved using

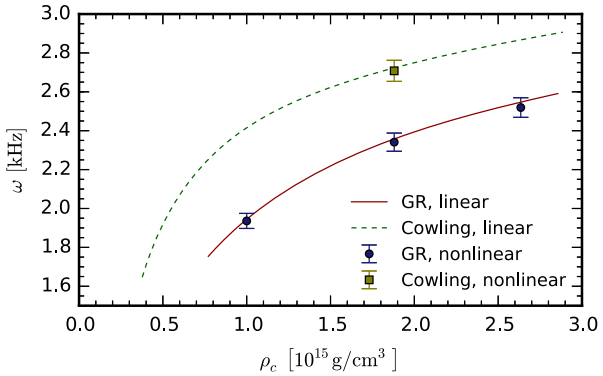

FIG. 8 (color online). The f-mode frequency ω for the SLy4 EOS, calculated with the linear codes in full GR and within the Cowling approximation, in comparison to results obtained with the three-dimensional nonlinear evolution code.

finite volume, high-resolution-shock-capturing methods. In particular, it employs piecewise parabolic reconstruction in conjunction with the HLLE approximate Riemann solver to compute fluxes. The spacetime is evolved by means of the publicly available McLachlan code [52], using the CCZ4 formulation of the metric evolution equations [53,54]. Note that we do not consider composition effects here, i.e., we ignore the electron fraction altogether and assume that the barotropic EOS which describes the background model is also valid during the evolution. The same assumption is implicitly made for the linear perturbation code.

The simulations made use of nested-box fixed mesh refinement with 6 refinement levels centered around the star. In this setup, the finest level fully contains the star, and the grid spacing is 222 m. We employ radiative boundary conditions for the metric at the outer boundary, which is located at 708 km.

Using this setup, we compared frequencies for three models with different central densities, all obeying the SLy EOS (chosen as a representative case). The results are shown in Fig. 8. We estimate the numerical errors (due to the numerical evolution and the resolution of the Fourier analysis used to extract the frequency) to be around 2%. The maximum difference between the frequencies obtained with the two codes is 1.1%. The results thus agree within the expected accuracy. We also computed the frequency for one model in the Cowling approximation. As shown in Fig. 8, the result matches the one using the linear code within 0.6%.

IV. CONCLUSIONS AND FINAL REMARKS

In this work, we provided accurate results for the f modes of neutron stars described by the 9 EOSs listed in Table I. Our results were obtained by solving the linear perturbation equations that describe the nonradial oscillations of relativistic neutron stars [39,40].

With these results, we were able to update the empirical fits proposed in the literature that describe the general behavior of the f-mode frequency ω and damping time τ as functions of the star's average density and compactness [19,20], based on the behavior of Newtonian stars and on the quadrupole formula, respectively.

Our results cover a comprehensive range of masses and contain more modern EOSs, allowing us to test proposed universal relations more stringently. In particular, we clearly showed that τ does not follow the linear fit proposed by [19]. We did however find a new universal relation for the quantity $\omega\tau$ as a function of the compactness, which describes our results more accurately. It can be used to restrict $\omega\tau$ from the compactness, but can only be inverted for low compactness. The more recent proposal in [21] for a universal relations describing the f modes in terms of the effective compactness still holds to very good accuracy for our set of EOS.

In our comparison with the results of a linear Cowling code, we confirmed previous results from [23] and extended them to more EOSs. The difference between the Cowling and the GR results ranges from ≈10–30% and decreases with increasing compactness.

Finally we compared our results with a three-dimensional nonlinear evolution code for a few stellar models employing the SLy4 EOS. We showed that the results agree well within the estimated error bars for the numerical results, thus validating the implementation of the different approaches presented here.

ACKNOWLEDGMENTS

This work was supported by CAPES and the Max Planck Society. Some of the computations were carried out on the Datura cluster of the AEI. We thank F. Galeazzi for preparing the LS220 and SHT EOS tables. C. Chirenti wishes to thank L. Rezzolla and S. Yoshida for useful discussions.

APPENDIX: NUMERICAL RESULTS FOR EACH EOS

In this appendix we present first numerical results for the f-mode frequency ω and damping time τ for a few representative stars generated with each one of the 9 EOS considered in this paper (see Table I). In addition, we provide mass, radius, and effective compactness η. These results are given in Tables III–XI.

TABLE III. Properties of selected models for the AkmalPR EOS. ρ_c is the central energy density, M is the gravitational mass, R the circumferential radius, η the effective compactness (dimensionless), ω is the frequency of the $m = 0, l = 2$ f mode, τ the corresponding damping time scale due to gravitational radiation. The first line refers to the most massive model.

ρ_c [10^{15} g/cm^3]	M [$M_\odot$]	R [km]	η	ω [kHz]	τ [s]
1.771	2.071	10.716	0.419	2.352	0.137
1.315	1.796	11.141	0.369	2.189	0.138
1.097	1.536	11.296	0.325	2.069	0.161
0.939	1.276	11.358	0.280	1.953	0.209
0.800	1.003	11.382	0.232	1.822	0.313

TABLE IV. Like Table III, but for the BalbN1H1 EOS.

ρ_c [10^{15} g/cm^3]	M [$M_\odot$]	R [km]	η	ω [kHz]	τ [s]
3.791	1.631	9.323	0.418	2.917	0.113
1.311	1.474	12.448	0.297	1.850	0.204
0.731	1.326	12.943	0.260	1.662	0.278
0.634	1.151	13.017	0.231	1.576	0.365
0.570	1.009	13.058	0.207	1.507	0.473

TABLE V. Like table III, but for the BBB2 EOS.

ρ_c [10^{15} g/cm^3]	M [$M_\odot$]	R [km]	η	ω [kHz]	τ [s]
3.189	1.921	9.500	0.439	2.733	0.133
1.619	1.696	10.686	0.369	2.313	0.130
1.245	1.457	11.066	0.319	2.114	0.161
1.011	1.231	11.260	0.275	1.958	0.216
0.847	1.028	11.350	0.236	1.830	0.303

TABLE VI. Like Table III, but for the BPAL12 EOS.

ρ_c [10^{15} g/cm^3]	M [$M_\odot$]	R [km]	η	ω [kHz]	τ [s]
3.981	1.455	9.013	0.395	2.991	0.104
1.954	1.339	10.515	0.325	2.362	0.144
1.477	1.223	11.102	0.289	2.122	0.187
1.209	1.120	11.504	0.260	1.958	0.240
1.000	1.011	11.866	0.233	1.809	0.317

TABLE VII. Like Table III, but for the FPS EOS.

ρ_c [10^{15} g/cm^3]	M [$M_\odot$]	R [km]	η	ω [kHz]	τ [s]
3.384	1.800	9.280	0.431	2.816	0.121
1.672	1.598	10.515	0.358	2.335	0.131
1.299	1.402	10.845	0.315	2.155	0.161
1.076	1.212	11.023	0.277	2.016	0.207
0.902	1.011	11.139	0.238	1.881	0.290

TABLE VIII. Like Table III, but for the GlendNH3 EOS.

ρ_c [10^{15} g/cm^3]	M [$M_\odot$]	R [km]	η	ω [kHz]	τ [s]
2.375	1.966	11.378	0.406	2.329	0.134
1.046	1.729	13.357	0.321	1.790	0.190
0.743	1.492	13.993	0.272	1.587	0.271
0.553	1.232	14.310	0.228	1.443	0.409
0.477	1.051	14.457	0.199	1.354	0.571

TABLE IX. Like Table III, but for the LS220 EOS.

ρ_c [10^{15} g/cm^3]	M [$M_\odot$]	R [km]	η	ω [kHz]	τ [s]
2.574	2.053	10.646	0.429	2.452	0.137
1.191	1.788	12.223	0.346	1.969	0.160
0.891	1.525	12.636	0.295	1.777	0.214
0.710	1.273	12.824	0.251	1.628	0.306
0.570	1.014	12.891	0.206	1.486	0.489

TABLE X. Like Table III, but for the SHT EOS.

ρ_c [10^{15} g/cm^3]	M [$M_\odot$]	R [km]	η	ω [kHz]	τ [s]
1.554	2.769	13.334	0.441	1.911	0.193
0.738	2.316	14.719	0.360	1.630	0.186
0.584	1.896	14.920	0.305	1.507	0.240
0.466	1.427	14.917	0.242	1.369	0.385
0.371	1.006	14.788	0.182	1.232	0.750

TABLE XI. Like Table III, but for the SLy4 EOS.

ρ_c [10^{15} g/cm^3]	M [$M_\odot$]	R [km]	η	ω [kHz]	τ [s]
2.856	2.049	9.992	0.443	2.591	0.144
1.417	1.793	11.284	0.368	2.183	0.138
1.084	1.517	11.635	0.316	2.001	0.172
0.896	1.273	11.791	0.272	1.865	0.230
0.771	1.068	11.866	0.236	1.754	0.316

[1] M. C. Miller, arXiv:1312.0029.
[2] A. Akmal, V. R. Pandharipande, and D. G. Ravenhall, Equation of state of nuclear matter and neutron star structure, Phys. Rev. C **58**, 1804 (1998).
[3] S. Balberg, G. R. Farrar, and T. Piran, Neutron stars with a stable, light supersymmetric baryon, Astrophys. J. **548**, L179 (2001).
[4] M. Baldo, I. Bombaci, and G. F. Burgio, Microscopic nuclear equation of state with three-body forces and neutron star structure, Astron. Astrophys. **328**, 274 (1997).
[5] I. Bombaci, M. Prakash, M. Prakash, P. J. Ellis, J. M. Lattimer, and G. E. Brown, Newborn hot neutron stars, Nucl. Phys. **A583**, 623 (1995).
[6] B. Friedman and V. R. Pandharipande, Hot and cold, nuclear and neutron matter, Nucl. Phys. **A361**, 502 (1981).
[7] N. K. Glendenning, Neutron stars are giant hypernuclei?, Astrophys. J. **293**, 470 (1985).
[8] F. Douchin and P. Haensel, A unified equation of state of dense matter and neutron star structure, Astron. Astrophys. **380**, 151 (2001).
[9] P. Haensel and B. Pichon, Experimental nuclear masses and the ground state of cold dense matter, Astron. Astrophys. **283**, 313 (1994).
[10] J. M. Lattimer and F. Douglas Swesty, A generalized equation of state for hot, dense matter, Nucl. Phys. **A535**, 331 (1991).
[11] G. Shen, C. J. Horowitz, and S. Teige, New equation of state for astrophysical simulations, Phys. Rev. C **83**, 035802 (2011).
[12] P. B. Demorest, T. Pennucci, S. M. Ransom, M. S. E. Roberts, and J. W. T. Hessels, A two-solar-mass neutron star measured using shapiro delay, Nature (London) **467**, 1081 (2010).
[13] J. Antoniadis *et al.*, A massive pulsar in a compact relativistic binary, Science **340**, 1233232 (2013).
[14] K. Yagi and N. Yunes, I-Love-Q Relations in neutron stars and their applications to astrophysics, gravitational waves and fundamental physics, Phys. Rev. D **88**, 023009 (2013).
[15] K. Yagi and N. Yunes, I-Love-Q: Unexpected universal relations for neutron stars and quark stars, Science **341**, 365 (2013).
[16] A. Maselli, V. Cardoso, V. Ferrari, L. Gualtieri, and P. Pani, Equation-of-state-independent relations in neutron stars, Phys. Rev. D **88**, 023007 (2013).
[17] M. Bejger and P. Haensel, Moments of inertia for neutron and strange stars: Limits derived for the crab pulsar, Astron. Astrophys. **396**, 917 (2002).
[18] J. M. Lattimer and B. F. Schutz, Constraining the equation of state with moment of inertia measurements, Astrophys. J. **629**, 979 (2005).
[19] N. Andersson and K. D. Kokkotas, Towards gravitational wave asteroseismology, Mon. Not. R. Astron. Soc. **299**, 1059 (1998).
[20] O. Benhar, V. Ferrari, and L. Gualtieri, Gravitational wave asteroseismology reexamined, Phys. Rev. D **70**, 124015 (2004).
[21] H. K. Lau, P. T. Leung, and L. M. Lin, Inferring physical parameters of compact stars from their f-mode gravitational wave signals, Astrophys. J. **714**, 1234 (2010).
[22] L. K. Tsui and P. T. Leung, Probing the Interior of Neutron Stars with Gravitational Waves, Phys. Rev. Lett. **95**, 151101 (2005).
[23] S. Yoshida and Y. Kojima, Accuracy of the relativistic cowling approximation in slowly rotating relativistic stars, Mon. Not. R. Astron. Soc. **289**, 117 (1997).
[24] C. Chirenti, J. Skákala, and S. Yoshida, Slowly rotating neutron stars with small differential rotation: equilibrium models and oscillations in the cowling approximation, Phys. Rev. D **87**, 044043 (2013).
[25] H. Sotani, K. D. Kokkotas, P. Laguna, and C. F. Sopuerta, Gravitationally driven electromagnetic perturbations of neutron stars and black holes, Phys. Rev. D **87**, 084018 (2013).
[26] H. Sotani, K. D. Kokkotas, P. Laguna, and C. F. Sopuerta, Electromagnetic waves from neutron stars and black holes driven by polar gravitational perturbations, Gen. Relativ. Gravit. **46**, 1675 (2014).
[27] A. L. Watts and T. E. Strohmayer, Detection with RHESSI of high-frequency x-ray oscillations in the tail of the 2004 hyperflare from SGR 180620, Astrophys. J. **637**, L117 (2006).
[28] A. Colaiuda, H. Beyer, and K. D. Kokkotas, On the quasi-periodic oscillations in magnetars, Mon. Not. R. Astron. Soc. **396**, 1441 (2009).
[29] K. D. Kokkotas and B. G. Schmidt, Quasi-normal modes of stars and black holes, Living Rev. Relativity **2**, 2 (1999).
[30] H. P. Nollert, Quasinormal modes: The characteristic "sound" of black holes and neutron stars, Classical Quantum Gravity **16**, R159 (1999).
[31] G. Allen, N. Andersson, K. D. Kokkotas, and B. F. Schutz, Gravitational waves from pulsating stars: Evolving the perturbation equations for a relativistic star, Phys. Rev. D **58**, 124012 (1998).
[32] W. Kastaun, B. Willburger, and K. D. Kokkotas, Saturation amplitude of the f-mode instability, Phys. Rev. D **82**, 104036 (2010).
[33] J. L. Friedman and B. F. Schutz, Secular instability of rotating Newtonian stars, Astrophys. J. **222**, 281 (1978).
[34] D. Doneva, E. Gaertig, K. D. Kokkotas, and C. Krger, Gravitational wave asteroseismology of fast rotating neutron stars with realistic equations of state, Phys. Rev. D **88**, 044052 (2013).
[35] E. B. Abdikamalov, H. Dimmelmeier, L. Rezzolla, and J. C. Miller, Relativistic simulations of the phase-transition-induced collapse of neutron stars, Mon. Not. R. Astron. Soc. **392**, 52 (2009).
[36] J. A. Pons, E. Berti, L. Gualtieri, G. Miniutti, and V. Ferrari, Gravitational signals emitted by a point mass orbiting a neutron star: Effects of stellar structure, Phys. Rev. D **65**, 104021 (2002).
[37] L. Baiotti, B. Giacomazzo, and L. Rezzolla, Accurate evolutions of inspiralling neutron-star binaries: Prompt and delayed collapse to black hole, Phys. Rev. D **78**, 084033 (2008).
[38] http://www.lorene.obspm.fr/.
[39] L. Lindblom and S. L. Detweiler, The quadrupole oscillations of neutron stars, Astrophys. J. **53**, 73 (1983).

[40] S. Detweiler and L. Lindblom, On the nonradial pulsations of general relativistic stellar models, Astrophys. J. **292**, 12 (1985).

[41] K. S. Thorne and A. Campolattaro, Non-radial pulsation of general-relativistic stellar models. I. Analytic analysis for $L \geq 2$, Astrophys. J. **149**, 591 (1967)

[42] R. Price and K. S. Thorne, Non-radial pulsation of general-relativistic stellar models. II. Properties of the gravitational waves, Astrophys. J. **155**, 163 (1969).

[43] K. S. Thorne, Non-radial pulsation of general-relativistic stellar models. III. Analytic and numerical results for neutron stars, Astrophys. J. **158**, 1 (1969).

[44] K. S. Thorne, Non-radial pulsation of general-relativistic stellar models. IV. The weak field limit, Astrophys. J. **158**, 997 (1969).

[45] A. Campolattaro and K. S. Thorne, Non-radial pulsation of general-relativistic stellar models. V. Analytic results for $L = 1$, Astrophys. J. **159**, 847 (1970).

[46] J. R. Ipser and K. S. Thorne, Non-radial pulsation of general-relativistic stellar models. VI. Corrections, Astrophys. J. **181**, 181 (1973).

[47] C. Chirenti, P. R. Silveira, and O. D. Aguiar, Non-radial oscillations of neutron stars and the detection of gravitational waves, Int. J. Mod. Phys. Conf. Ser. **18**, 48 (2012).

[48] F. Galeazzi, W. Kastaun, L. Rezzolla, and J. A. Font, Implementation of a simplified approach to radiative transfer in general relativity, Phys. Rev. D **88**, 064009 (2013).

[49] H. Dimmelmeier, N. Stergioulas, and J. A. Font, Non-linear axisymmetric pulsations of rotating relativistic stars in the conformal flatness approximation, Mon. Not. R. Astron. Soc. **368**, 1609 (2006).

[50] W. Kastaun, Inertial modes of rigidly rotating neutron stars in cowling approximation, Phys. Rev. D **77**, 124019 (2008).

[51] S. Yoshida and Y. Eriguchi, Neutral points of oscillation modes along equilibrium sequences of rapidly rotating polytropes in general relativity: Application of the cowling approximation, Astrophys. J. **490**, 779 (1997).

[52] D. Brown, P. Diener, O. Sarbach, E. Schnetter, and M. Tiglio, Turduckening black holes: An analytical and computational study, Phys. Rev. D **79**, 044023 (2009).

[53] D. Alic, C. Bona-Casas, C. Bona, L. Rezzolla, and C. Palenzuela, Conformal and covariant formulation of the Z4 system with constraint-violation damping, Phys. Rev. D **85**, 064040 (2012).

[54] D. Alic, W. Kastaun, and L. Rezzolla, Constraint damping of the conformal and covariant formulation of the Z4 system in simulations of binary neutron stars, Phys. Rev. D **88**, 064049 (2013).